Electronic Supplementary Material (ESI) for ChemComm.

Supporting Information

Self-assembled anion channel formation by bis(1,3-propanediol)-linked meta-dipropynylbenzenebis(1,3-diol)-based small molecules

Rashmi Sharma, Amal Vijay, Sandip Chattopadhayay, Arnab Mukherjee* and Pinaki Talukdar *

Table of Content

I. General Methods

All reactions were carried out under the nitrogen atmosphere. All the chemicals were purchased from commercial sources and were used as received unless stated otherwise. Solvents were dried by standard methods prior to use or purchased as dry. Thin layer chromatography (TLC) was carried out with E. Merck silica gel 60-F_{254} plates and column chromatography was performed over silica gel (100-200 mesh) obtained from commercial suppliers. Egg yolk phosphatidylcholine (EYPC) lipid was purchased from Avanti Polar Lipids as a solution dissolved in chloroform (25 mg/mL). HEPES buffer, HPTS dye, ANTS-DPX system, Triton X-100, NaOH, and all inorganic salts of molecular biology grade were purchased from Sigma. Gel-permeation chromatography was performed on a column of Sephadex LH-20 gel (25×300 mm,

V_0 = 25 mL). Large unilamellar vesicles (LUV) were prepared from EYPC lipid by using a mini extruder, equipped with a polycarbonate membrane either of 100 nm or 200 nm pore size, obtained from Avanti Polar Lipids.

II. Physical Measurements

The ^{1}H and ^{13}C NMR spectra were recorded on 400 MHz Jeol ECS-400 (or 101 MHz for ^{13}C) spectrometers using either residual solvent signals as an internal reference or from internal tetramethylsilane on the δ scale relative to chloroform (δ 7.26 ppm), dimethylsulphoxide (δ 2.50 ppm), acetone (δ 2.05 ppm) for ^{1}H NMR and chloroform (δ 77.20 ppm), dimethylsulphoxide (δ 39.50 ppm), acetone (δ 29.84 and 206.26 ppm) for ^{13}C NMR. The chemical shifts (δ) are reported in ppm and coupling constants (J) in Hz. The following abbreviations are used: s (singlet), d (doublet) m (multiplet), and td (triplet of doublet) while describing ^{1}H NMR signals. High-resolution mass spectra (HRMS) were obtained from the MicroMass ESI-TOF MS spectrometer. Fluorescence spectra were recorded by using Fluoromax-4 from Jobin Yvon Edison equipped with an injector port and a magnetic stirrer. 10 mM HEPES (with 100 mM NaCl or other salts as per necessity) buffer solutions were used for the fluorescence experiment and the pH of the buffers was adjusted to 7.0 or 8.0 by NaOH and the pH of the buffer solutions was measured using Helmer pH meter. FT-IR spectra were obtained using NICOLET 6700 FT-IR spectrophotometer as KBr disc and reported in cm^{-1}. Melting points of all the compounds were measured using a VEEGO Melting point apparatus. All melting points were measured in open glass capillary and values are uncorrected. All fluorescence data were processed either by Origin 8.5 or Kaleida Graph and finally, all data were processed through Chem Draw Professional 15.

III. Synthesis

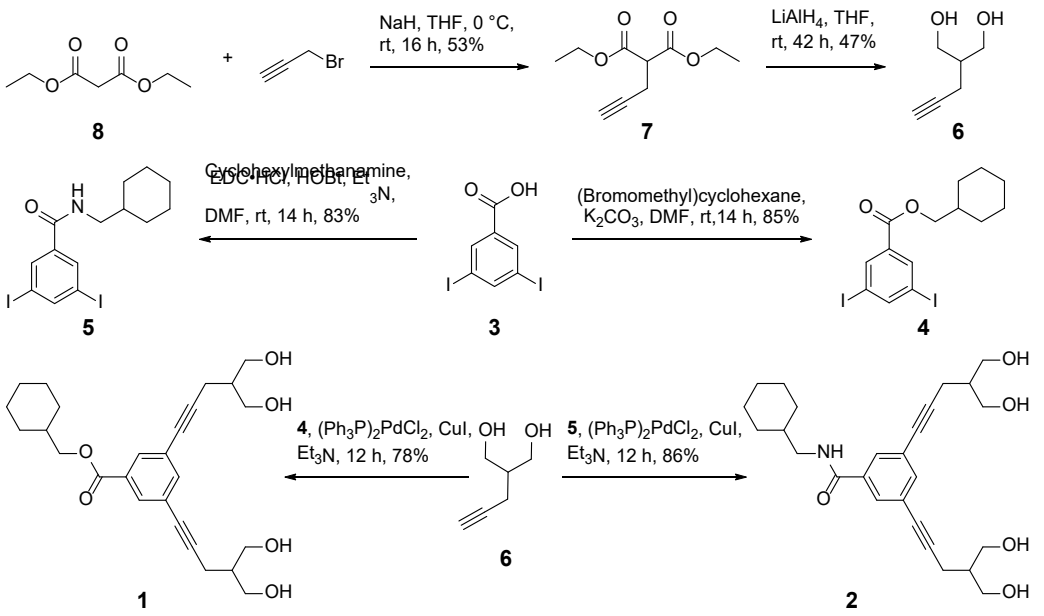

Scheme S1. Synthesis of bis-1,3-diol ester derivative **1** and amide derivative **2**.

Synthesis of *diethyl 2-(prop-2-yn-1-yl) malonate*, 7, $C_{10}H_{14}O_4$: Compound **7** was synthesized by a reported protocol.[S1] The product was purified by column chromatography (SiO_2, EtOAc/C_6H_{14} = 5:95 – 10:90) to yield product **7,** diethyl 2-(prop-2-yn-1-yl) malonate as transparent liquid (Yield = 53%). **^{1}H NMR** (400 MHz δ, $CDCl_3$): δ 1.28 (t, 6H); 2.01 (t, 1H); 2.78 (dd, 2H); 3.56 (t, 1H); 4.23 (m, 4H). Characterization data of the synthesized compound was matched with reported data.[S1]

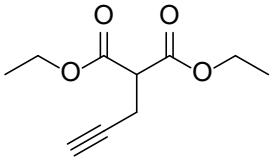

Synthesis of *2-(prop-2-yn-1-yl) propane-1,3-diol*, 6, $C_6H_{10}O_2$: Compound **6** was synthesized by a reported protocol. The product was purified by column chromatography (SiO_2, $CHCl_3$/MeOH = 5:95 – 10:90) to yield the product **6**, 2-(prop-2-yn-1-yl) propane-1,3-diol as transparent viscous liquid (Yield = 47%). **^{1}H NMR** (400 MHz δ, $CDCl_3$): δ 3.64 (m, 4H); 2.3 (dd, 2H); 2.26 (t, 1H); 1.86 (m, 1H). Characterization data of the synthesized compound was matched with reported data.[S1]

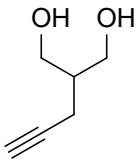

Synthesis of *3,5-diiodobenzoic acid*, 3, $C_7H_4I_2O_2$: Compound **3** was synthesized by a reported protocol.[S2] The crude product **3**, 3,5 – diiodobenzoic acid was purified by column chromatography (SiO_2, $CHCl_3$/MeOH = 5:95 – 8:92) to give a white solid (Yield = 62.6%). **^{1}H NMR** (400 MHz, DMSO-d_6): δ 13.53 (s, 1H), 8.35 (t, J= 1.5 Hz,

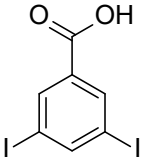

1H), 8.19 (d, J= 1.5 Hz, 2H). Characterization data of the synthesized compound was matched with reported data.[S2]

Synthesis of *cyclohexyl methyl 3,5-diiodobenzoate*, 4, $C_{14}H_{16}I_2O_2$: 3,5- diiodobenzoic acid, **3** (500 mg, 1.33 mmol, 1 equiv.) and K_2CO_3 (462 mg, 3.34 mmol, 2 equiv.) were stirred in DMF under nitrogen atmosphere. After, that bromomethyl cyclohexane (474 mg, 0.38 mL, 3.34 mmol, 2.5 equiv.) was added to it and kept on stirring overnight at room temperature.[S3] Completion of the reaction was monitored by Thin Layer Chromatography (TLC). The reaction mixture was partitioned between ethyl acetate (organic phase, 50 mL each time) and brine solution (aqueous phase). Three repetitions of extraction followed by drying of the combined organic layer over anhydrous sodium sulfate were done. The solvent was evaporated under reduced pressure. The crude product **4**, cyclohexylmethyl 3,5-diiodobenzoate was purified by column chromatography (SiO_2, $CHCl_3$/MeOH = 3:97 – 5:95) to yield the viscous liquid (Yield = 43.72 %). **^{1}H NMR** (400 MHz δ, $CDCl_3$): δ 8.29 (d, J= 8.3 Hz, 2H); 8.22 (t, J = 8.22 Hz, 1H); 4.12 (d, J = 4.12 Hz, 2H); 1.81 – 1.72 (m, 7H); 1.3 – 1.2 (m, 4H). **^{13}C NMR** (101 MHz δ, $CDCl_3$): δ 163.92, 149.23, 137.79, 133.82, 94.53, 71, 37.24, 29.82, 26.44, 25.75. **IR** (neat, ν/cm^{-1}) 3428, 3071, 2923, 2851, 2111, 1721, 1545, 1451, 1414, 1254, 1120, 976, 874, 761, 709, 661, 556.

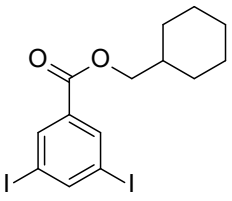

Synthesis of *N-(cyclohexylmethyl)-3,5-diiodobenzamide*, 5, $C_{14}H_{17}I_2NO$: 3,5-diiodobenzoic acid, **4** (500 mg, 1.33 mmol, 1 equiv.), EDC·HCl (568 mg, 4.00 mmol, 3 equiv.) and HOBT (495 mg, 3.2 mmol, 2.4 equiv.) were added to an oven-dried 100 mL round bottom flask under a nitrogen atmosphere. After that triethylamine (0.8 mL, 5.89 mmol, 2.5 equiv.) and then DMF (10 mL) was added to the flask. Finally, cyclohexylmethylamine (0.3 mL, 2 mmol, 1.5 equiv.) was added dropwise to the round bottom flask. Then the round bottom flask was left, stirring overnight.[S4] Completion of the reaction was monitored using Thin Layer Chromatography (TLC). The reaction mixture was partitioned between ethyl acetate (organic phase, 50 mL each time) and brine solution (aqueous phase) in a separating funnel, and the organic layer was extracted three times. The combined organic layer was dried over anhydrous sodium sulfate and the solvent was removed under reduced pressure. The crude product **5**, N-(cyclohexylmethyl)-3,5-diiodobenzamide was purified by column chromatography (SiO_2, $CHCl_3$/MeOH = 3:97 – 5:95) to yield colorless solid (Yield = 83%). **^{1}H NMR** (400 MHz δ, $CDCl_3$): δ 8.16 (t, J = 8.16 Hz, 1H); 8.01(d, J = 8.01 Hz, 2H); 6.07 (s, 1H); 3.26 (t, J = 3.28 Hz, 2H); 1.77 – 1.73 (m, 5H);

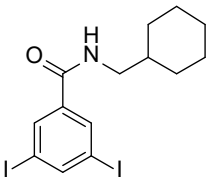

1.26 – 1.20 (m, 6H). **^{13}C NMR** (101 MHz δ, $CDCl_3$): δ 166.89, 137.9, 134.52, 128.64, 98.3, 46.45, 38.14, 31.06, 26.51, 25.94. **IR** (neat, ν/cm^{-1}) 3886, 3840, 3723, 3673, 3606, 3256, 3070, 2916, 2850, 2315, 1728, 1621, 1531, 1437, 1359, 1306, 1269, 1214, 1142, 1026, 962, 901, 859, 778, 730, 692, 553.

Synthesis of *cyclohexylmethyl 3,5-bis(5-hydroxy-4-(hydroxymethyl)pent-1-yn-1- yl)benzoate*:, 1, $C_{26}H_{34}O_6$: Cyclohexylmethyl 3,5-diiodobenzoate **6** (100 mg, 0.21 mmol, 1 equiv.) was taken in a 100 mL round bottom flask and triethyl amine (4 – 5 mL) was added to it. The round bottom flask was degassed for 30 – 40 minutes by bubbling nitrogen gas through the mixture. Then $PdCl_2(PPh_3)_2$ (5 mg, 0.01 mmol, 0.08 equiv.), CuI (4 mg, 0.02 mmol, 0.11 equiv.) and compound **3** (92 mg, 0.8 mmol, 3 equiv.) were added one by one to the solution in the round bottom flask containing Compound **6.** The solution was stirred for about 6 h after which the completion of the reaction was monitored by Thin Layer Chromatography (TLC).[S5] The reaction mixture was partitioned between ethyl acetate (organic phase, 50 mL each time) and brine solution (aqueous phase) in a separating funnel, and the organic layer was extracted three times. The combined organic layer was dried over anhydrous sodium sulfate and the solvent was removed under reduced pressure. The product **1**, cyclohexylmethyl 3,5-bis(5-hydroxy-4-(hydroxymethyl)pent-1-yn-1-yl)benzoate was purified by column chromatography (SiO_2, $CHCl_3$/MeOH = 1:99 – 5:95) to yield a viscous liquid (Yield = 78%). **^{1}H NMR** (400 MHz δ, $CDCl_3$): δ 7.89 (d, J = 7.89 Hz, 2H); 7.54 (t, J = 7.55 Hz, 1H); 4.10 (d, J = 4.10 Hz, 2H); 3.91 – 3.81 (m, 8H); 2.74 (s, 4H); 2.53 (d, J = 2.53 Hz, 4H); 2.09 – 2.03 (m, 2H); 1.77 – 1.73 (m, 7H); 1.26 – 1.20 (m, 2H); 1.07 – 1.00 (m, 2H). **^{13}C NMR** (101 MHz δ, $CDCl_3$): δ 165.71, 138.66, 131.73, 131.03, 124.32, 89.46, 80.65, 41.84, 37.29, 29.87, 26.48, 25.80, 18.55. **IR** (neat, ν/cm^{-1}) 3388, 2928, 2858, 2314, 2232, 1707, 1444, 1390, 1337, 1230, 1108, 1023, 894., 729, 608, 555, 516; **HRMS (ESI):** Calcd. $C_{26}H_{34}O_6$ $[M+H]^+$: 443.2355, Found: 443.2357.

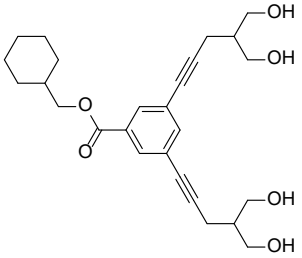

Synthesis of *N-(cyclohexylmethyl)-3,5-bis(5-hydroxy-4-(hydroxymethyl) pent-1-yn-1-yl)benzamide*, 2, $C_{26}H_{35}NO_5$: N-(cyclohexylmethyl)-3,5-diiodobenzamide, **5** (150 mg, 0.32 mmol, 1 equiv.) was taken in a 100 mL round bottom flask and triethyl amine (4 – 5 mL) was added to it. The round bottom flask was degassed for 30 – 40 minutes by bubbling nitrogen gas through the mixture. Then $PdCl_2(PPh_3)_2$ (7 mg, 0.01 mmol, 0.032 equiv.), CuI (6 mg, 0.03 mmol, 0.11 equiv.) and compound **3** (164 mg, 1.44 mmol, 4.5 equiv.) were

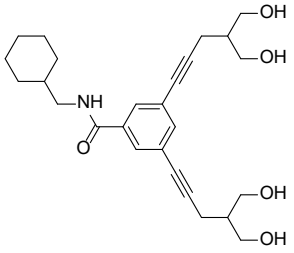

added one by one to the solution in the round bottom flask containing compound **5.** The solution was stirred for about 6 hours after which the completion of the reaction was monitored by Thin Layer Chromatography (TLC).[S5] The reaction mixture was partitioned between ethyl acetate (organic phase, 50 mL each time) and brine solution (aqueous phase) in a separating funnel, and the organic layer was extracted three times. The combined organic layer was dried over anhydrous sodium sulfate and the solvent was removed under reduced pressure. The product **2** was purified by column chromatography (SiO_2, $CHCl_3$/MeOH = 1:99 – 5:95) to yield product N-(cyclohexylmethyl)-3,5-bis(5-hydroxy-4-(hydroxymethyl) pent-1-yn-1-yl)benzamide, **2** as a light brown solid (Yield = 86%). **^{1}H NMR** (400 MHz δ, MeOH–d_4) 7.73 (d, J = 7.73 Hz, 2H); 7.49 (t, J = 7.5 Hz, 1H); 3.73 – 3.64 (m, 8H); 3.61 – 3.55 (m, 1H); 3.18 (d, J = 3.18 Hz, 2H); 2.55 (d, J = 2.55 Hz, 4H); 1.97 – 1.91 (m, 2H); 1.78 – 1.73 (m, 5H); 1.29 – 1.23 (m, 4H); 1.02 – 0.96 (m, 2H). **^{13}C NMR** (101 MHz δ, $CDCl_3$): δ 136.95, 135.22, 124.49, 129.39, 89.56, 80.58, 64.04, 46.57, 41.92, 38.08, 30.99, 26.53, 25.95, 18.45. **IR** (neat, ν/cm^{-1}): 3360, 2926, 2722, 2166, 1639, 1546, 1448, 1267, 1030, 893.14, 729.25. **HRMS (ESI):** Calcd. $C_{26}H_{34}O_6$ $[M+H]^+$: 442.2515, Found: 442.2519.

IV. SCXRD

The needle-shaped crystals of compound **2** were grown in a solvent combination of MeOH/CH_2Cl_2 at room temperature. The single-crystal X-ray data of compound **2** was recorded at 150 K on a Bruker KAPPA APEX II CCD Duo diffractometer (operated at 1500 W power: 50 kV, 30 mA) using graphite-mono chromated Mo Kα radiation (λ = 0.71073 Å). The crystal was kept on a nylon Cryo-Loops (Hampton Research) with Paraton-N (Hampton Research). The data reduction and integration were computed with SAINT software.[S6] A correction on multi-scan absorption was employed on the collected reflections. The structure solving was achieved by the direct method using SHELXTL[S7] and was further refined on *F*2 by full-matrix least-squares technique using the SHELXL-97[S8] program package within the WINGX[S9] program. All the non-hydrogen atoms were refined anisotropically. All hydrogen atoms were located in successive difference Fourier maps, and they were treated as riding atoms using SHELXL default parameters. The structures were examined using the *Adsym* subroutine of PLATON[S10] to ensure that no additional symmetry could be applied to the models.

Crystallographic data for compound **2**: **CCDC 2192071** contains the supplementary crystallographic data for this paper and can be obtained free of charge from The Cambridge Crystallographic Data Centre.

Table S1. Crystal data and structure refinement for Compound2.

Identification code	**Compound2**
CCDC Number	**2192071**
Empirical formula	$C_{26}H_{35}NO_5$
Formula weight	441.55
Temperature	296(2) K
Wavelength	1.54178 Å
Crystal system	Triclinic
Space group	P-1
Unit cell dimensions	a = 5.146(2) Å α= 82.17(3)°. b = 11.099(5) Å β= 85.54(3)°. c = 20.771(8) Å γ = 88.37(3)°.
Volume	1171.6(8) $Å^3$
Z	2
Density (calculated)	1.252 Mg/m^3
Absorption coefficient	0.692 mm^{-1}
F(000)	476
Crystal size	0.300 x 0.100 x 0.100 mm^3
Theta range for data collection	2.153 to 60.000°.
Index ranges	-5<=h<=5, -12<=k<=10, -23<=l<=23
Reflections collected	7019
Independent reflections	3112 [R(int) = 0.1431]
Completeness to theta = 60.000°	89.4 %
Absorption correction	Semi-empirical from equivalents
Max. and min. transmission	0.91 and 0.70
Refinement method	Full-matrix least-squares on F^2
Data / restraints / parameters	3112 / 1221 / 475
Goodness-of-fit on F^2	1.341
Final R indices [I>2sigma(I)]	R1 = 0.1390, wR2 = 0.3637
R indices (all data)	R1 = 0.2521, wR2 = 0.4229
Extinction coefficient	0.032(7)
Largest diff. peak and hole	0.848 and -0.505 $e.Å^{-3}$

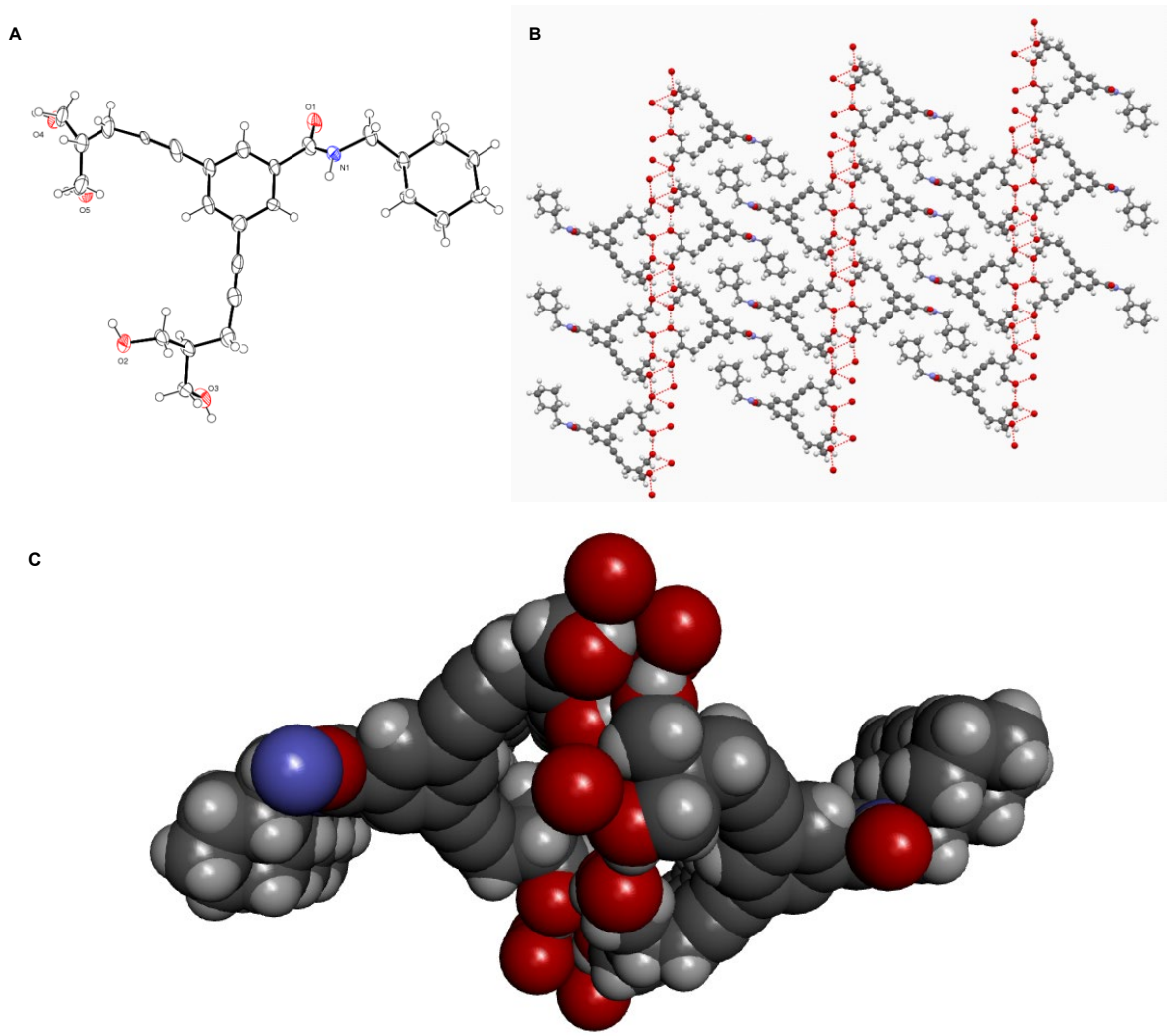

Fig. S1 ORTEP diagram of **2** (**A**). Hydrogen bonded network of **2** in the solid state (**B**). Three molecules are stacked in two adjacent layers facing each other in the space fill model for **2** (along a-axis). (**C**).

V. Ion Transport Experiments[S11]

A. Ion transporting activity studies across EYPC–LUVs ⊃ HPTS:

Preparation of HEPES buffer and stock solutions: The HEPES buffer of pH = 7.0 was prepared by dissolving an appropriate amount of solid HEPES (10 mM) and NaCl (100 mM) in autoclaved water. The pH was adjusted to 7.0 by adding aliquots from 0.5 M NaOH solution. The stock solution of all carriers was prepared using HPLC grade DMSO.

Preparation of EYPC–LUVs ⊃ HPTS in NaCl: The vesicles were prepared by the reported protocol.[S14-S16]

Ion transport activity by HPTS assay: In clean and dry fluorescence cuvette, 1975 µL of HEPES buffer (10 mM HEPES, 100 mM NaCl, pH =7.0) and 25 µL of EYPC–LUVs⊃HPTS vesicle was added. The cuvette was placed in a slowly stirring condition using a magnetic stirrer equipped in a fluorescence instrument (t = 0 s). The time-dependent HPTS emission intensity was monitored at λ_{em} = 510 nm (λ_{ex} = 450 nm) by creating a pH gradient between intra and extra vesicular system by the addition of 0.5 M NaOH (20 µL) at t = 20 s. Then different concentrations of transporter molecules in DMSO were added at t = 100 s. Finally, the vesicle was lysed by the addition of 10% Triton X–100 (25 µL) at t = 300 s to disrupt the pH gradient (Fig. S2). The time-dependent data were normalized to percent change in fluorescence intensity using Equation S1:

$$I_F = [(I_t - I_0)/ (I_\infty - I_0)] \times 100) \qquad \text{(Equation S1)}$$

where I_0 is the initial intensity, I_t is the intensity at time t, and I_∞ is the final intensity after the addition of Triton X–100.

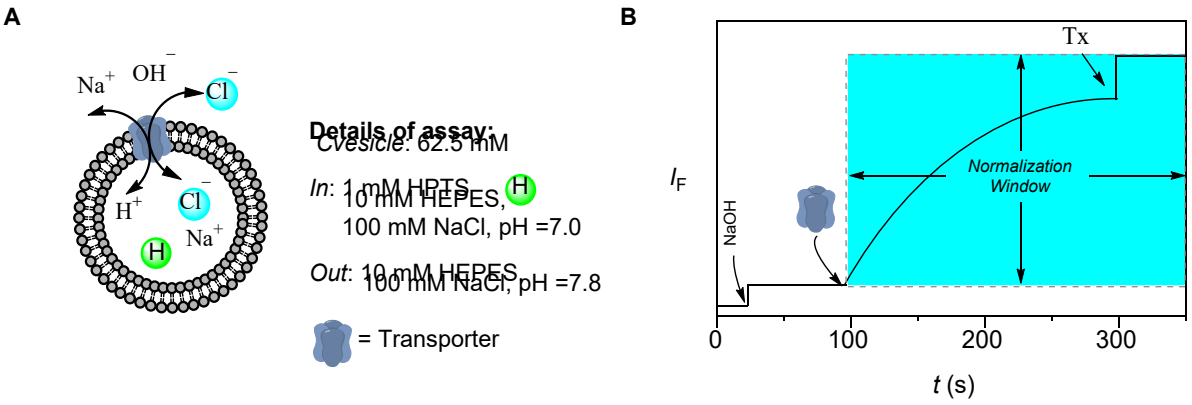

Fig. S2 Representations of fluorescence-based ion transport activity assay using EYPC–LUVs⊃HPTS (**A**), and illustration of ion transport kinetics showing normalization window (**B**).

Dose-response activity:

The fluorescence kinetics of each transporter at different concentrations was studied as the course of time. The concentration profile data were evaluated at t = 170 s to get effective concentration, EC_{50} (i.e. the concentration of transporter needed to achieve 50% chloride efflux)[S12] using Hill equation (Equation S2):

$$Y = Y_\infty + (Y_0 - Y_\infty)/[1 + (c/EC_{50})^n \qquad \text{(Equation S2)}$$

where, Y_0 = fluorescence intensity just before the transporter addition (at t = 0 s), Y_∞ = fluorescence intensity with excess transporter concentration, c = concentration of transporter

compound, and n = Hill coefficient (i.e. indicative of the number of monomers needed to form an active supramolecular channel).[S13]

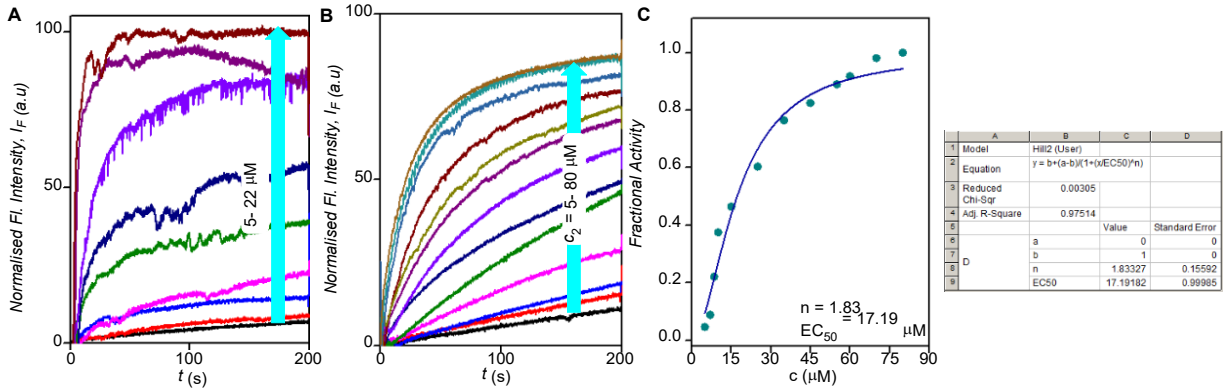

Fig. S3 Dose-response curve of (**A**) ester **1**, (**B**) amide **2**, derivative and (**C**) Hill analysis of compound **2** at 170 s.

The concentration profile data were analyzed by Hill Equation (Equation S2) to get the Effective concentration (EC_{50}) and Hill coefficient (n), (Fig. S3)

$$Y = Y_\infty + (Y_0 - Y_\infty) / [1 + (c / EC_{50})^n] \qquad \text{(Equation S2)}$$

where, Y_0 = Fluorescence intensity just before the channel addition (at 0 s). Y_∞ = Fluorescence intensity with excess channel concentration, c = Concentration of channel forming molecule.

B. Ion selectivity studies across EYPC–LUVs⊃HPTS:

Preparation of EYPC–LUVs ⊃ HPTS: The vesicles were prepared by the following reported protocol.[S14-S16]

Preparation of buffer and stock solutions: The HEPES buffer solution of 10 mM HEPES and 100 mM salts were prepared by dissolving appropriate amounts of solid HEPES and salts (NaCl, NaF, NaBr, $NaNO_3$, NaOAc, LiCl, KCl, RbCl, and CsCl) in autoclaved water, followed by adjustment of pH = 7.0 using 0.5 M NaOH. The stock solution of the most active transporter was prepared in HPLC grade DMSO.

Anion selectivity assay: In a clean and dry fluorescence cuvette 1975 µL HEPES buffer (10 mM HEPES, 100 mM NaX, pH = 7.0; where X = F^-, Cl^-, Br^-, OAc^-, and NO_3^-) was taken, followed by the addition of 25 µL EYPC–LUVs⊃HPTS. The resulting solution was slowly stirred in a fluorescence instrument equipped with the magnetic stirrer (t = 0 s). The fluorescence intensity of HPTS was observed at λ_{em} = 510 nm (λ_{ex} = 450 nm) over a course of time, by creating pH gradient by addition of 20 µL 0.5 M NaOH at t = 20 s, followed by the addition of transporter **2** (as a DMSO solution) at t = 100 s to initiate ion transport and finally, vesicle was lysed for

complete disruption of pH gradient by addition of 25 µL 10% Triton X – 100 at t = 300 s. The time-dependent data were normalized to percent change in intensity using Equation S1

Cation selectivity assay: In a similar way, cation selectivity of transporter **2** (as a DMSO solution) was explored by changing extravesicular HEPES buffer solution (10 mM HEPES, 100 mM MCl, pH = 7.0) of chloride salts (MCl) of different cation (M = Li^+, Na^+, K^+, Rb^+, Cs^+). Using the same condition, no difference in fluorescence intensity was observed for different cations. The fluorescence data was normalised to percent change in intensity over course of time using Equation S1.

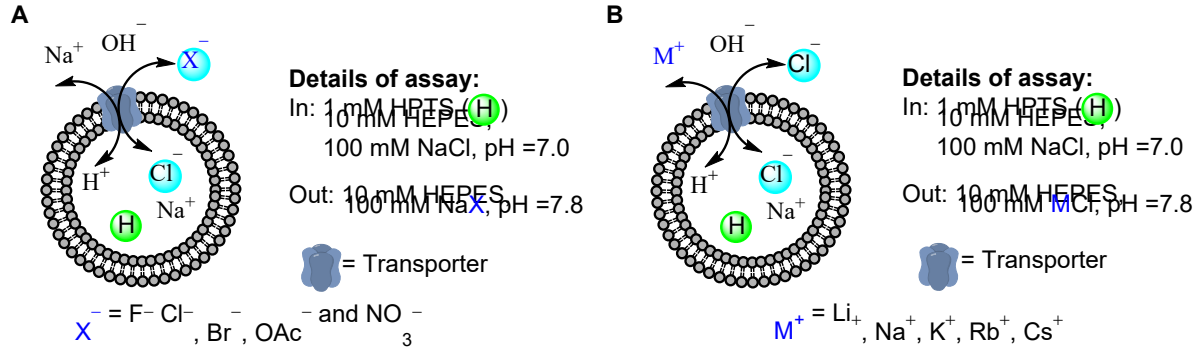

Fig. S4 Schematic representations of fluorescence-based anion **(A)** and cation selectivity **(B)** assays.

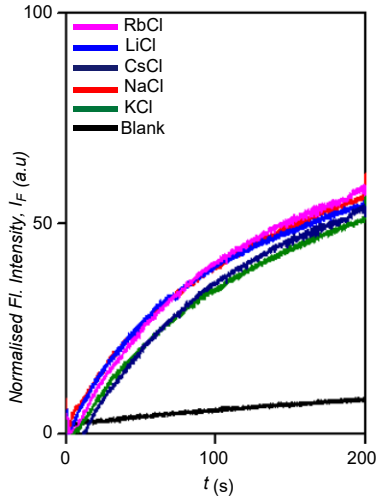

Fig. S5 Cation selectivity of **2** at 17 µM.

C. Ion transport activity across EYPC–LUVs⊃HPTS in presence of valinomycin:[S17,S18]

In a clean fluorimetric cuvette 1975 µL of buffer solution (100 mM KCl, 10 mM HEPES, pH 7.0), 25 µL of above prepared vesicles solution were taken and placed in a fluorescence instrument equipped with a magnetic stirrer at t = 0 s. The fluorescence emission intensity of the HPTS dye, It was measured at λ_{em} = 510 nm (where λ_{ex} = 450 nm) for the time course of 0 to

350 s. At t = 20 s, 20 µL of 0.5 M NaOH solution was added to the same cuvette to generate a pH gradient (ΔpH = 0.8) between intra and extra vesicular medium. Then valinomycin (2.5 pM) was added at t = 50s followed by the addition of 18 µL solution of **2** in DMSO at t = 100 s. At t = 300 s, 25 µL of 10% triton X-100 was added to destroy all the vesicles for destructing the pH gradient. All the data was normalized using the Eq. S1.

Comparable rates of pH gradient collapse were found when the ion transport activity of **2** was measured in the absence and presence of valinomycin. Therefore, the experiments indicated preferential selectivity of **2** towards Cl^- over OH^-, i.e., $Cl^- \gg OH^-$.

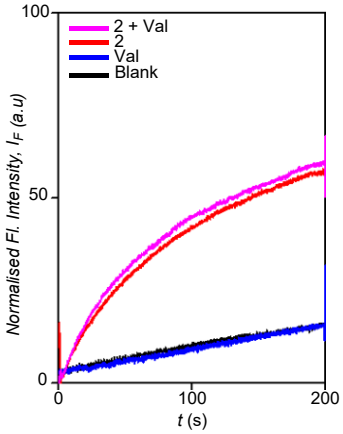

Fig. S6 Ion transport activity of **2** (18 µM) determined across EYPC–LUVs⊃HPTS in the absence and presence of valinomycin.

D. Chloride transport activity across EYPC–LUVs⊃lucigenin vesicles:

Preparation of EYPC–LUVs⊃lucigenin vesicles:

The vesicles were prepared by the reported protocol.[S14-S16]

Ion transport activity by Lucigenin assay:

In clean and dry fluorescence cuvette 1975 µL 200 mM $NaNO_3$ solution and 25 µL EYPC–LUVs⊃lucigenin was taken. This suspension was placed in a slowly stirring condition in fluorescence instrument equipped with a magnetic stirrer (at t = 0 s). The fluorescence intensity of lucigenin was monitored at λ_{em} = 535 nm (λ_{ex} = 450 nm) over a course of time. The chloride gradient was created by the addition of 33.3 µL NaCl (2.0 M) at t = 20 s between the intra and extra vesicular system, followed by the addition of a transporter at t = 100 s. Finally, vesicles were lysed by the addition of Triton X–100 at t = 300 s for the complete disruption of the chloride gradient.

The time-dependent data were normalized to percent change in fluorescence intensity using Equation S3:

$$I_F = [(I_t - I_0) / (I_\infty - I_0)] \times -100) \qquad \text{(Equation S3)}$$

Where, I_0 is the initial intensity, I_t is the intensity at time t, and I_∞ is the final intensity after the addition of Triton X–100.

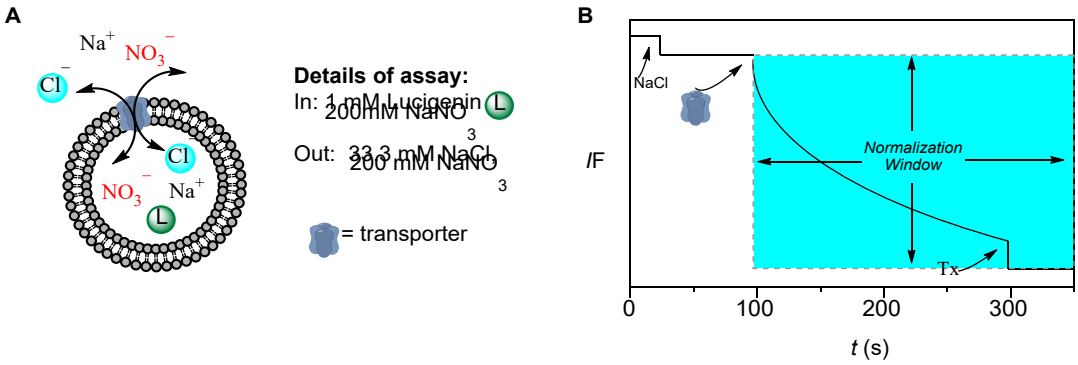

Fig. S7 Representations of fluorescence-based ion transport activity assay using EYPC–LUVs⊃ Lucigenin (**A**), and illustration of ion transport kinetics showing normalization window (**B**).

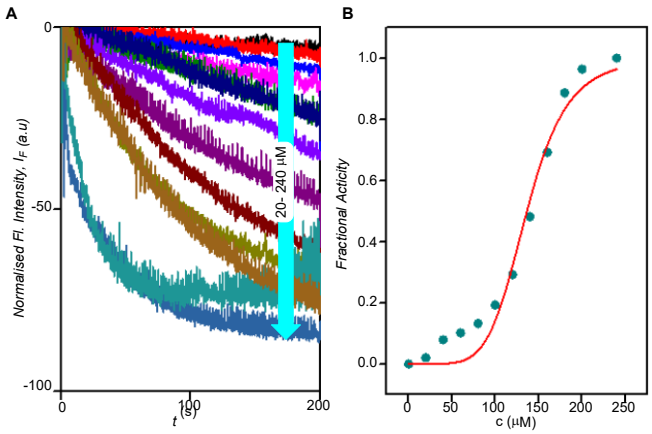

Fig. S8 Concentration dependent activity of compound **2** across EYPC–LUVs⊃lucigenin (**A**). Hill plot analysis of compound **2** (**B**).

Involvement of cation in transport process:

The involvement of cations in the transport process was evaluated from the lucigenin-based assay. The preparation of solutions and vesicles are similar as described in the above section. In assay condition, the chloride salt of various cation ($M^+ = Li^+$, Na^+, K^+, Rb^+ and Cs^+) were added to evaluate the contribution of cation in transport process.

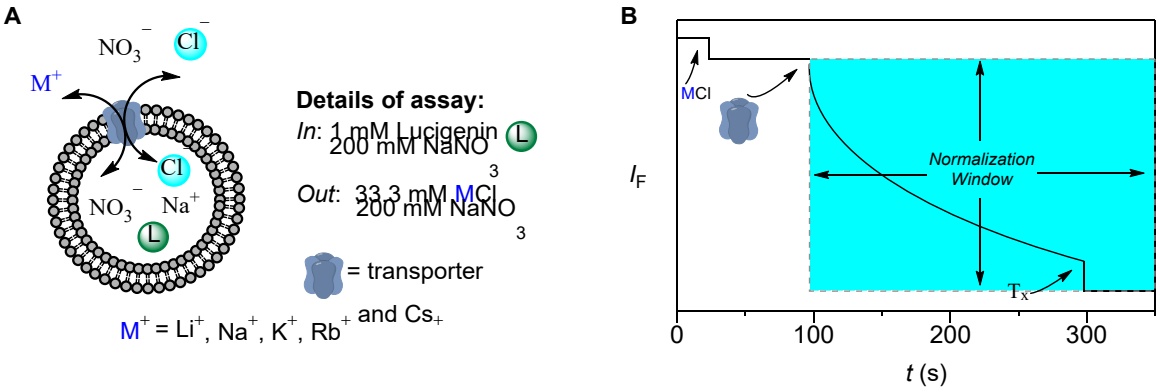

Fig. S9 Representations of chloride influx activity assay using EYPC–LUVs⊃ Lucigenin by varying extravesicular cations (**A**), and illustration of chloride influx kinetics showing normalization window (**B**).

Cation transport activity: In a clean and dry fluorescence cuvette 1975 µL of $NaNO_3$ solution (200 mM) was added followed by the addition of 25 µL of EYPC–LUVs⊃lucigenin. The cuvette was placed in the fluorescence instrument in a slowly stirring condition by a magnetic stirrer equipped with the instrument (at t = 0 s). The time course of lucigenin fluorescence emission intensity, F_t was observed at λ_{em} = 535 nm (λ_{ex} = 450 nm). 33.3 µL of 2 M, MCl ($M^+ = Li^+$, Na^+, K^+, Rb^+ and Cs^+) was added to the cuvette at t = 25 s to create the chloride gradient between the intra and extra vesicular system. Transporter molecule **2** was added at t = 100 s in different concentrations and, finally, 25 µL of 10% Triton X–100 was added at t = 300 s to lyse those vesicles resulting destruction of the chloride gradient (Fig. S9, S10).

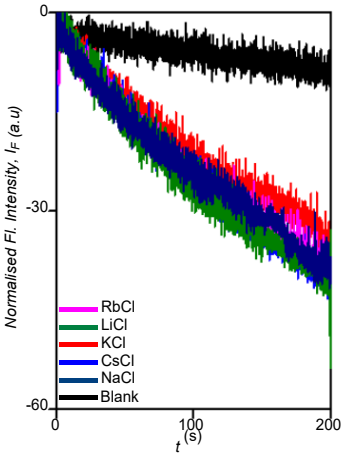

Fig. S10 Influence of extravesicular cations in the Cl^- influx by **2** at 22 µM.

Ion transport activity across EYPC–LUVs⊃lucigenin in the presence of valinomycin: The antiport mechanism (i.e. simultaneous transport of two different ions, in opposite directions, across the membrane)[S11] of **2** was experimentally confirmed by lucigenin assay in the presence of valinomycin. The ion transport activity of **2** was monitored in vesicle entrapped with lucigenin

(1 mM) and $NaNO_3$ (200 mM) suspended in KCl (2 M) solution with and without valinomycin. The remarkable enhancement in ion transport activity of **2** in the presence of valinomycin gave direct experimental insight into the antiport mechanism of ion transport. Preparation of EYPC–LUVs⊃lucigenin: The vesicles were prepared by the protocol.[S14-S16]

Antiport mechanism: In clean and dry fluorescence cuvette 1975 µL 200 mM $NaNO_3$ solution and 25 µL EYPC–LUVs⊃lucigenin vesicles were taken and slowly stirred in a fluorescence instrument equipped with a magnetic stirrer (at t = 0 s). The time-dependent fluorescence intensity of lucigenin was monitored at λ_{em} = 535 nm (λ_{ex} = 455 nm). A solution of 2 M KCl (33.3 µL) was added at t = 20 s to create a chloride gradient between intra and extra vesicular system, followed by the addition of valinomycin (1.25 µM) at t = 50 s and transporter **2** (1.25 µM) at t = 100 s. Finally, the destruction of the chloride gradient was done by the addition of 10 % Triton X–100 (25 µL) at t = 300 s (Fig. S11). The time-dependent data were normalized to percent change in fluorescence intensity using Equation S3.

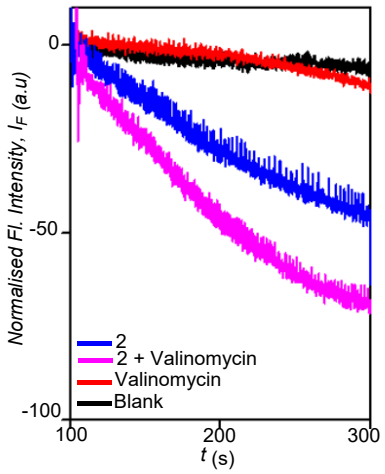

Fig. S11 Comparison of Cl^- influx activity of **2** in the absence and in the presence of valinomycin (1.25 µM).

E. Transporter Mechanism (Cholesterol Method):

The fluidity of the EYPC/cholesterol membrane changes when the amount of cholesterol in it changes, and this should have an impact on carriers by altering their mobility. However, since transmembrane channels span the entire membrane, they shouldn't be impacted. Increasing cholesterol levels will lower the membrane's fluidity to slow down a carrier's rate of transit but won't show any change in the fluorescence of the channel.[S19]

Vesicles were prepared as before, but with 10 mol% of cholesterol added during the initial stage of vesicle preparation.[S20]

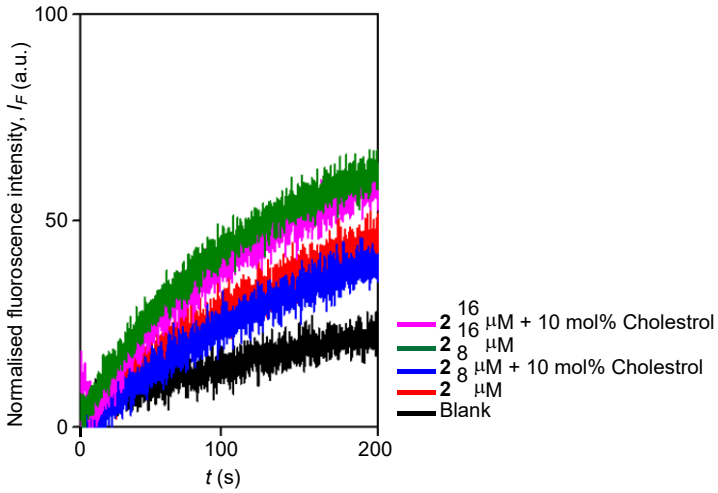

Fig. S12 Effect of the amount of cholesterol in the EYPC/cholesterol membrane on transport by 2 (10 mol%, of cholesterol in the membrane).

F. Evaluation of membrane stability and channel nature by ANTS-DPX assay: EYPC–LUVs were loaded with anionic fluorophore ANTS (8-aminonaphthalene-1,3,6-trisulfonic acid disodium salt) and cationic quencher DPX (1,1-[1,4 phenylenebis(methylene)]bis[pyridinium]bromide) (Fig. S13). Efflux of either ANTS or DPX through pores formed by **1** or **2** was followed by an increase in ANTS emission intensity.

The following buffers were prepared by a known method.

Buffer A: 12.5 mM ANTS, 45.0 mM DPX, 5 mM TES, 20 mM KCl, pH = 7.0

Buffer B: 5 mM TES, 100 mM KCl, pH = 7.0.

Preparation of EYPC–LUVs⊃ ANTS/DPX vesicles: A thin film of EYPC lipid was prepared by evaporating a solution (1 mL) of EYPC lipid (25 mg/mL) in $CHCl_3$ evaporated slowly by a stream of nitrogen and then in vacuo (6 h), and then hydrated with 1 mL buffer A, followed by vortex treatment (4 times). The resulting suspension was subjected to > 5 freeze-thaw cycles (using liquid N_2 to freeze and a warm water bath to thaw), and 19 times extruded using a Mini-Extruder through a 100 nm polycarbonate membrane (Avanti). External ANTS/DPX was removed by gel filtration (Sephadex G-50) using buffer B and diluted with the same buffer to 3 mL to give EYPC-LUVs⊃ ANTS/DPX stock solution.

ANTS/DPX assay: In a clean and dry fluorescence cuvette, 50 μL of the above lipid solution and 1950 μL buffer B were added. The compound **1** or **2** were added at 50 s and kept in a slowly stirring condition by a magnetic stirrer equipped with the fluorescence instrument (at t = 0 s).

The time course of fluorescence emission intensity, F_t was monitored at λ_{em} = 520 nm (λ_{ex} = 353 nm).

Finally, at t = 300 s, 25 µL of 10% Triton X–100 was added to lyse all vesicles for 100% dye efflux. Fluorescence intensities (F_t) were normalized to fractional emission intensity I_F using Equation S2.

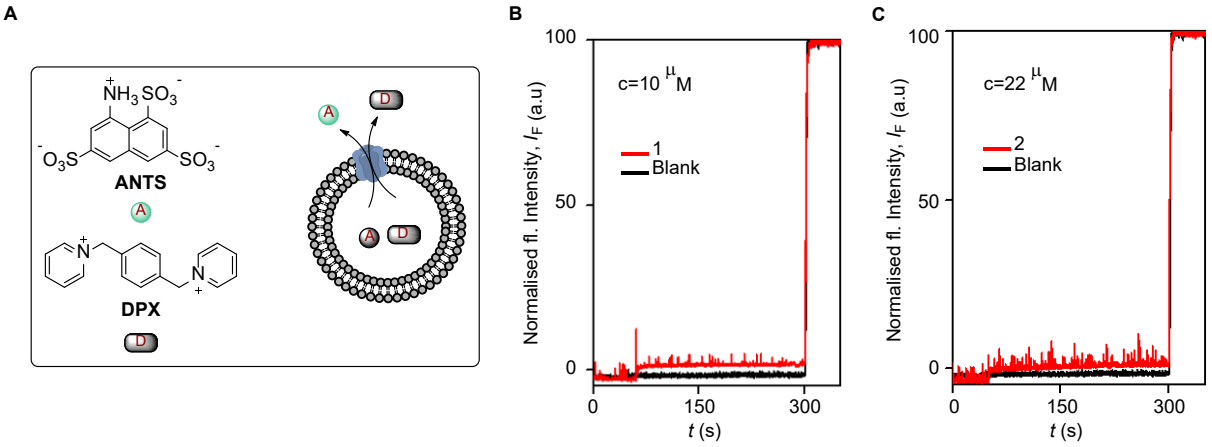

Fig. S13 Representation of ANTS–DPX assay **(A)** and ANTS–DPX leakage assay in presence of compound **1** (**B**) and compound **2** (**C**).

VI. Planar Bilayer Conductance Measurements[S21]

Bilayer membrane (BLM) was formed across an aperture of 150 µM diameter in a polystyrene cup (Warner Instrument, USA) with lipid diphytanoylphosphatidylcholine (Avanti Polar Lipids), dissolved in *n*-decane (18 mg/mL). Both chambers (*cis* and *trans*) were filled with symmetrical solution, containing 1 M KCl. The *trans* compartment was held at virtual ground and the *cis* chamber was connected to the BC 535 head-stage (Warner Instrument, USA) via matched Ag–AgCl electrodes. Compound **2** (10 µM) was added to the *trans* chamber and the solution was stirred with a magnetic stirrer for 30 min. Channel formation was confirmed by the distinctive channel opening and closing events after applying voltages. Currents were low pass filtered at 1 kHz using pClamp9 software (Molecular Probes, USA) and an analog-to-digital converter (Digidata 1440, Molecular Probes). All data were analyzed by the software pClamp 9.

The complete data trace observed for 10 min contained a series of opening and closing events at some indefinite intervals. From a large and complete trace, a small portion is presented in the manuscript (Fig. 4A, B). The average current was calculated from this trace and then conductance and other calculations were made accordingly.

Calculation of ion channel diameter: Diameter of artificial ion channel was calculated according to Hille's equation,

$$1/g = (l + \pi d/4) \times (4\rho/\pi d^2) \qquad \text{(Equation S5)}$$

Where, g = corrected conductance (obtained by multiplying measured conductance with the Sansom's correction factor) = 3.37×10^{-10} S, l = length of the ion channel = 34 Å, and ρ = resistivity of the 1 M KCl solution = 9.47 Ω·cm).

Anion selectivity by Planar Bilayer Conductance Measurements:

The *cis* and *trans* chambers were filled with unsymmetric solutions of KCl. The *cis* chamber was filled with 0.5 M KCl solution and the *trans* chamber was filled with 1 M KCl. The compound **2** (10 µM) was added to the *trans* chamber and stirred for 20 min. The reversal potential was calculated to be –20 ± 2 mV.

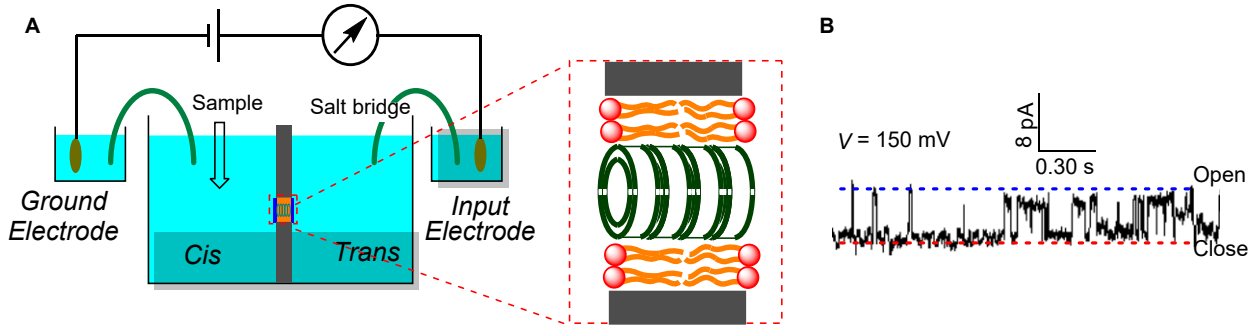

Fig. S14 Systematic representation of black lipid membrane experiment **(A)** and Single-channel conductance of **2** (10 µM) recorded (A) at +150 mV **(B)**.

VII. Theoretical Studies

System Preparation: Single channel-membrane system is constructed by embedding the quantum mechanically optimized synthetic ion channel in the DPHPC membrane and solvated it by 10586 water molecules, 63 Na^+ and 63 Cl^- ions (corresponding to 200 mM concentration). To solvate the system, ~11000 SPC model[S22] water molecules were added to the system. The pre-equilibrated structure and parameters for DPHPC (1,2-diphytanoyl-sn-glycero-3-phosphocholine) obtained from Lipidbook [S23]. The optimized channel was placed in the box of 128 DPHPC molecules using inflategro methodology [S24]. The automated topology builder [S25] created by Malde, et al. was used to develop the all-atom topology parameters of the channel with GROMOS-53a6 force field [S26]. Molecular dynamics simulation was carried out using GROMACS 2019.6 [S27] package.

Molecular Dynamics simulation details: The system was minimized using the steepest descent method for 50000 steps. This was followed by equilibration for 10 ns at constant temperature for

323 K temperature and 1 bar pressure using Nosé-Hoover thermostat [S28] and Parrinello-Rahman barostat [S29] with a coupling constant of 0.5 ps and 5 ps, respectively. The time step of each simulation was taken as 2 fs. PME electrostatics [S30] was used for electrostatic interactions using a 12Å cut-off with the van der Waals (vdW) cut-off set at 12 Å. Position restraints of 500 kJ/mol nm^2 were applied to the heavy atoms of the channel molecules. The simulation box was found to be approximately 7.0X7.4X10.0 nm^3 for the system. A final 50 ns molecular dynamics simulation at constant 323 K temperature and 1 bar pressure was carried out using Nosé-Hoover thermostat [S28] and Parrinello-Rahman barostat [S29] with a coupling constant of 0.5 ps and 2 ps respectively with similar electrostatics and vdW as in equilibration process.

Free energy calculations for permeation events: we used state-of-the-art multiple walker metadynamics[S31] simulations by positioning a reference chloride ion at various parts of the channel. The initial configurations for constructing the multiple walker metadynamics simulation setup is obtained from the permeation event captured from the unbiased MD simulation trajectory. In this enhanced sampling approach, independent biased simulations are considered in parallel, and the bias contribution from each walker are considered for constructing the final free energy surface for the permeation process, till the last ion is out from the channel. A total of 8 walkers were constructed (each sampling different independent trajectory) and a total of 160 ns simulations (20 ns each) were performed using the Z-Coordinate (displacement of Cl^- ion along Z-coordinate, hereafter referred as permeation distance) between the channel and reference chloride ion as a collective variable (CV) to study the permeation events. This CV quantitatively describe the position of ion inside and outside the channel in the simulation system. Near the centre the channel, the permeation distance have the value of 0 nm and when it reaches the bulk water it has a value greater than 2.5 nm. We considered a hill height of 0.2 kJ/mol, a bias factor of 10, and hills deposition rate of 1 ps and Gaussian widths of 0.05 nm for the metadynamics simulation.

Calculation of coordination number: The coordination number between the Cl^- ion and water molecules is calculated using the switching function described as follows Group A contains the reference chloride ion and Group B contains the oxygen atoms of the water molecules present in the system.

$$Coord.Number = \sum_{i \in A} \sum_{i \in B} s_{ij}$$

$$s_{ij} = \frac{1 - \left(\frac{r_{ij} - d_0}{r_0}\right)^n}{1 - \left(\frac{r_{ij} - d_0}{r_0}\right)^m}$$

r_{ij} describes the distance between the reference chloride ion and the neighbouring oxygen atoms of the water molecules. r_0 and d_0 values set to 0.35 nm and 0 nm respectively.

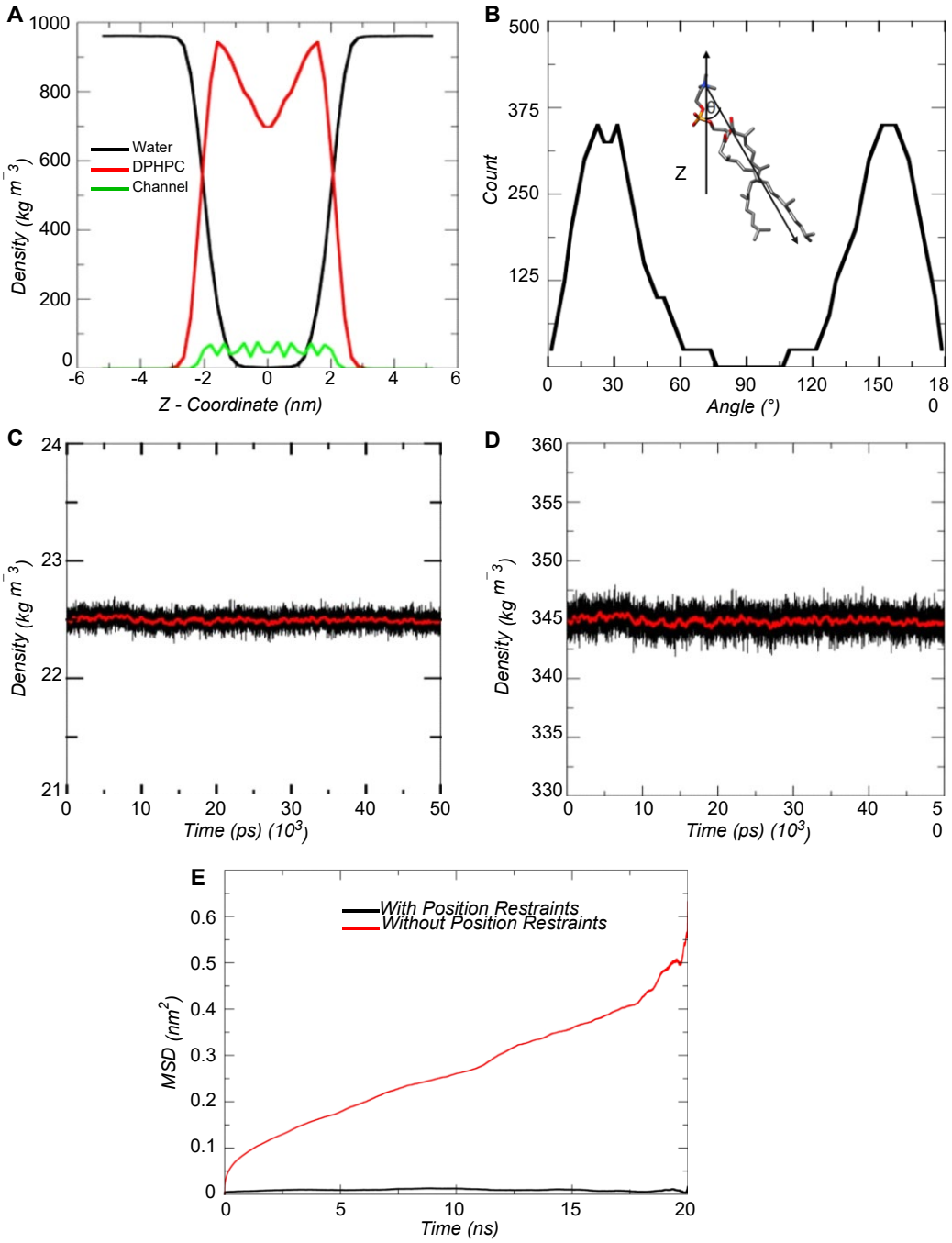

Fig. S15 Partial density profile of water, DPHPC, and channel present in the system with respect to Z – coordinate **(A)**, Distribution of angle formed by channel axis (Z – direction) and a vector connecting the head group to the long tail end of the alkyl group of the DPHPC. The figure shows two clear peaks near 20° to 32° and 150° to 160°, corresponding to two oppositely oriented molecules in two layers **(B)**, time evolution of the density of channel present in the system **(C)**, time evolution of the density of DPHPC present in the system **(D).** Comparison of mean square displacement (MSD) profiles of the channel with and without position restraints in the initial 20 ns simulations of the production run. It is found that the channel atoms move in the absence of position restraints. Hence, we have used the trajectory of the system with position restraints applied to the channel for all analysis and free energy calculations **(E)**.

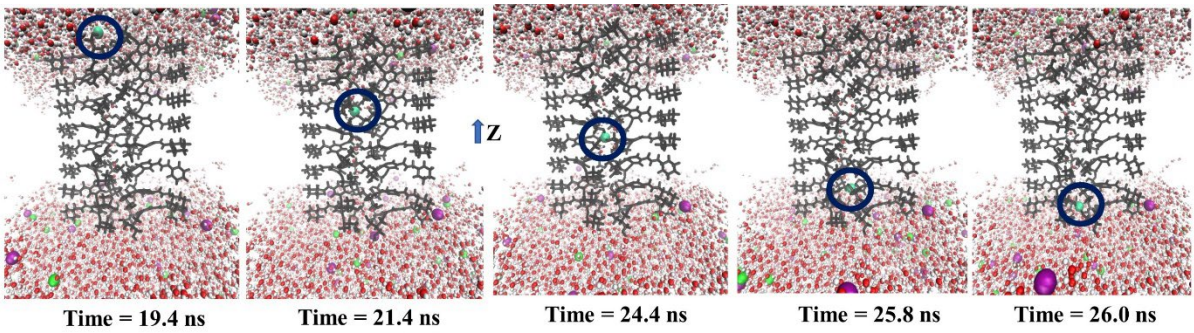

Fig. S16 A closer view of channel in black (lipid molecules omitted for clarity), water molecules (red), sodium ion (purple), and chloride ions (green; permeating ion is encircled in blue) at different timepoint.

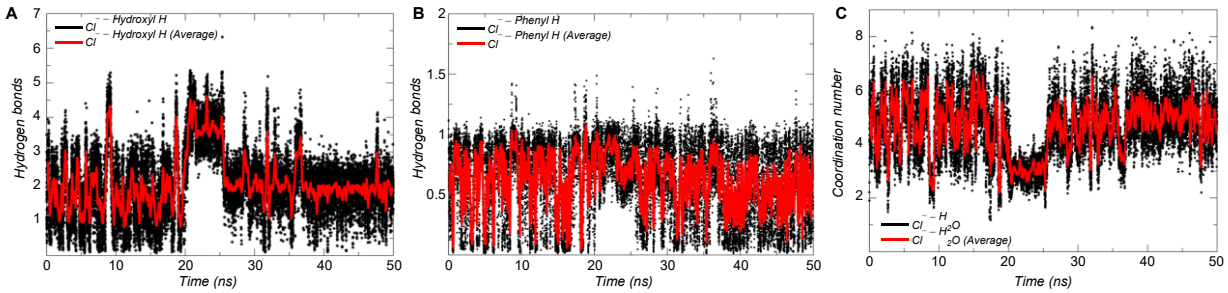

Fig. S17 Evolution of closest chloride ion (with respect to virtual centre of the channel) permeated through the channel. Variation of Hydrogen bonds between Hydroxyl group and chloride ion with respect to time **(A)**, the variation of hydrogen bonds between phenyl hydrogens and the chloride ion with respect to time **(B)** and the variation in the coordination number between chloride ion and water molecules with respect to time **(C)**.

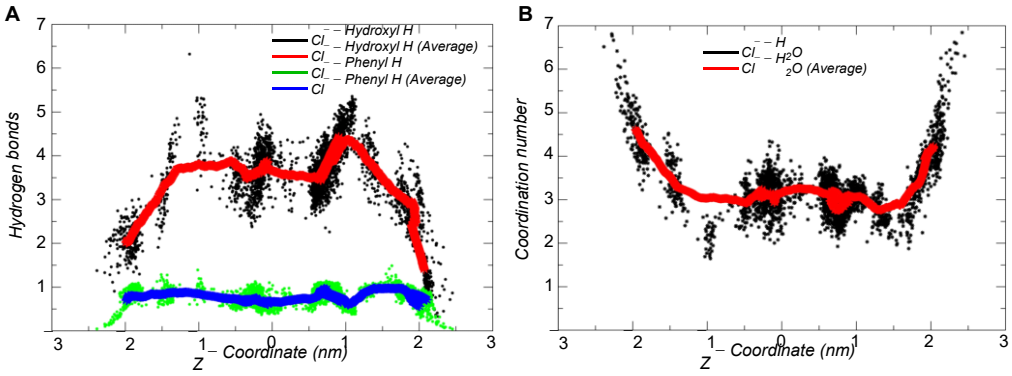

Fig. S18 Variation of hydrogen bonds between the permeated chloride ions with hydroxyl groups of channel and phenyl hydrogens. The starting and ending residues of the channel have the values –2.2 nm and 2.2 nm respectively **(A)** and variation of coordination number between chloride ion and water molecule in the system during the permeation pathway **(B)**.

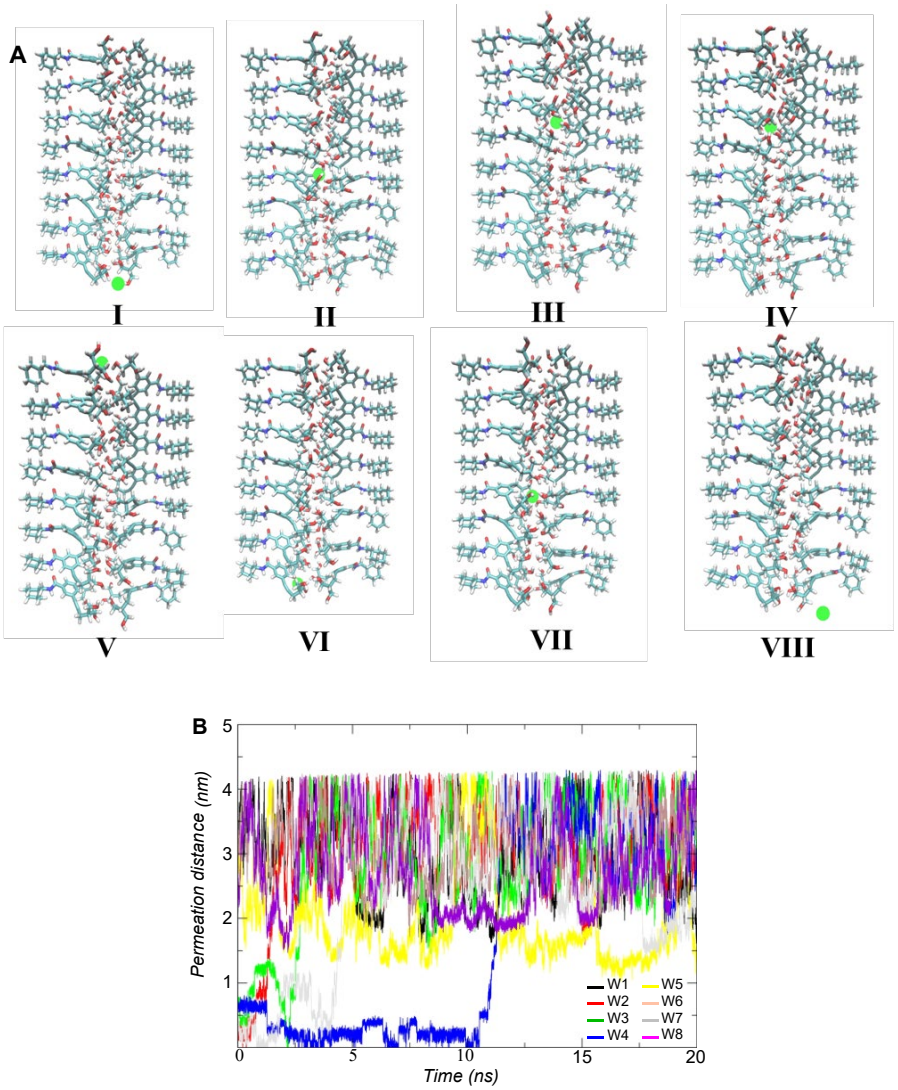

Fig. S19 Structure of Cl^- and channel in the system used as initial configuration for multiple-walker metadynamics simulation. The starting geometry with reference Cl^- ion (green) of each of these walkers is shown. **(A)**. Variation of permeation distance with respect to time for each of the walker used for the simulation. The colour code for each of the walker is shown in the inset **(B)**.

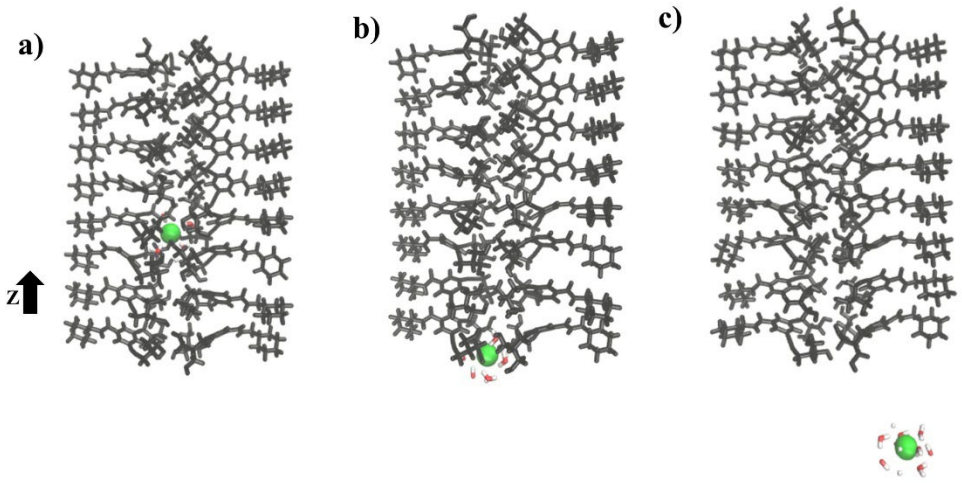

Fig. S20 Structural representation of minima states, corresponding to the permeation of chloride ion from free energy plots shown in Fig. 4c. Cl^- ion is shown green colour with surrounded water molecules (red colour). minima state "A" (permeated state) **(A)**, minima state "B" (Transition state) **(B)**, and minima state "C" (Free state) **(C)**.

VIII. NMR Spectra

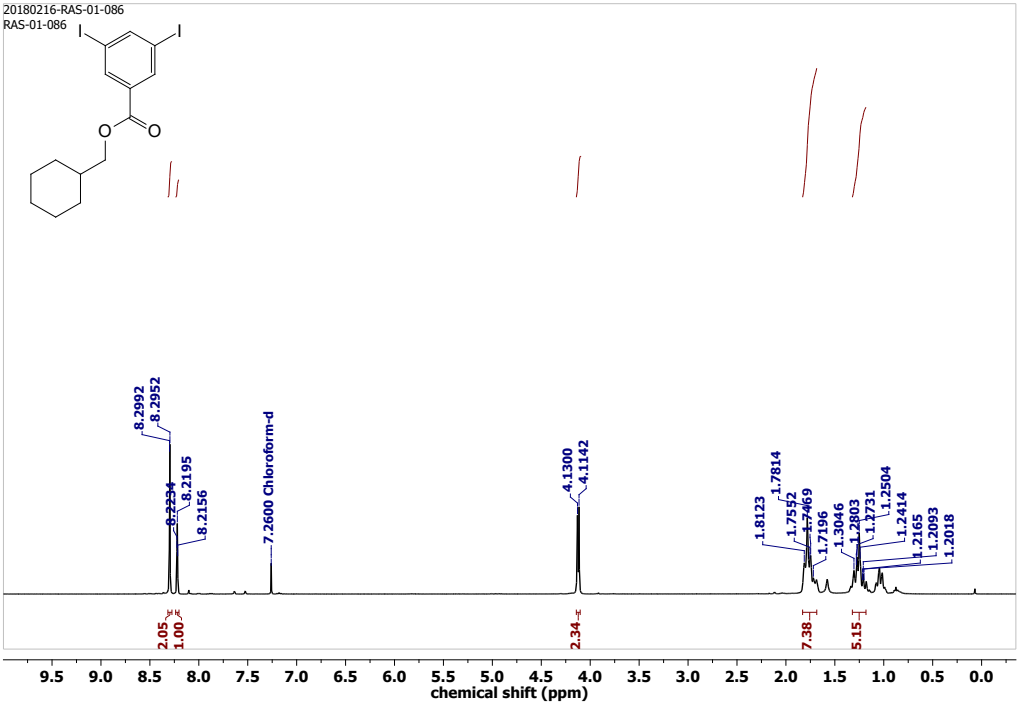

Fig. S21 ^{1}H NMR (400 MHz) spectrum of **4** in $CDCl_3$.

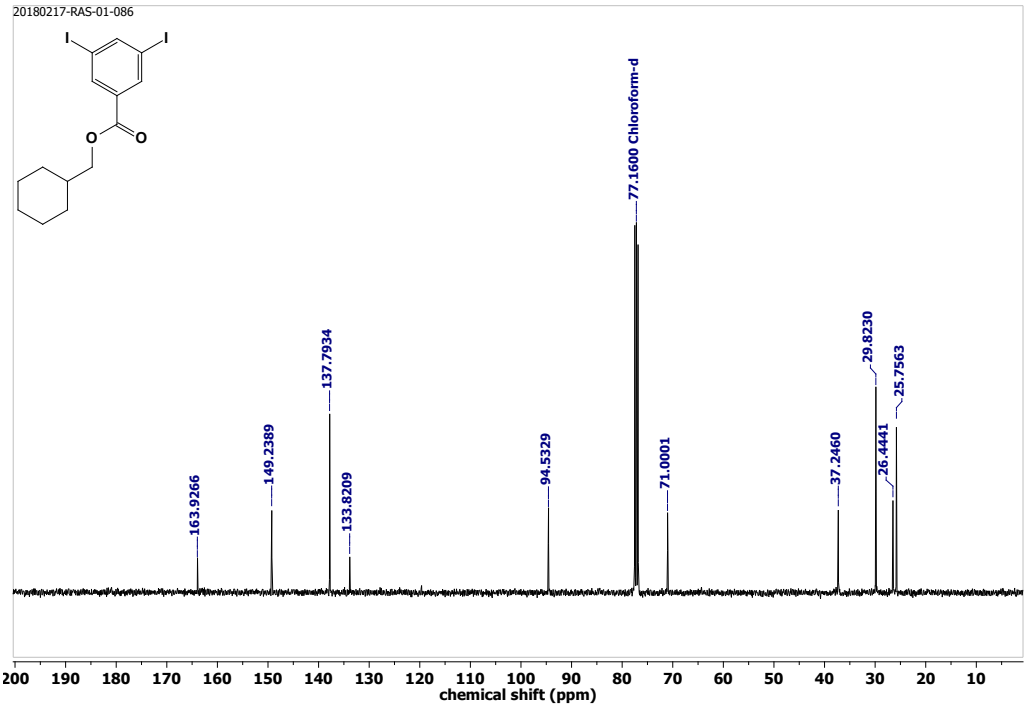

Fig. S22 ^{13}C NMR (101 MHz) spectrum of **4** in $CDCl_3$.

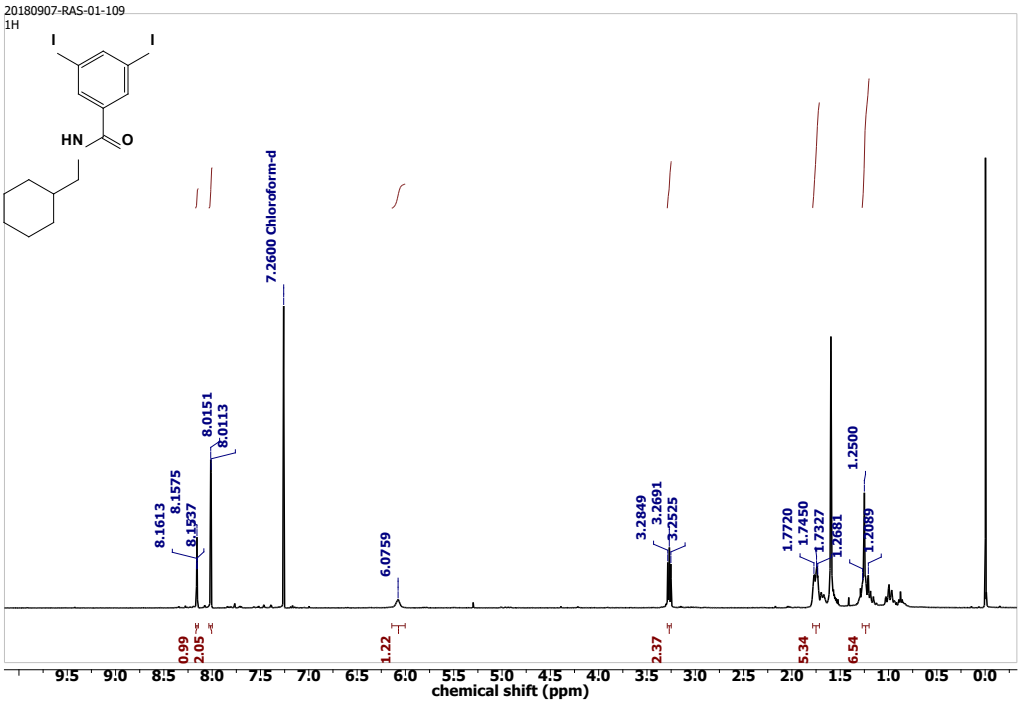

Fig. S23 ^{1}H NMR (400 MHz) spectrum of **5** in $CDCl_3$.

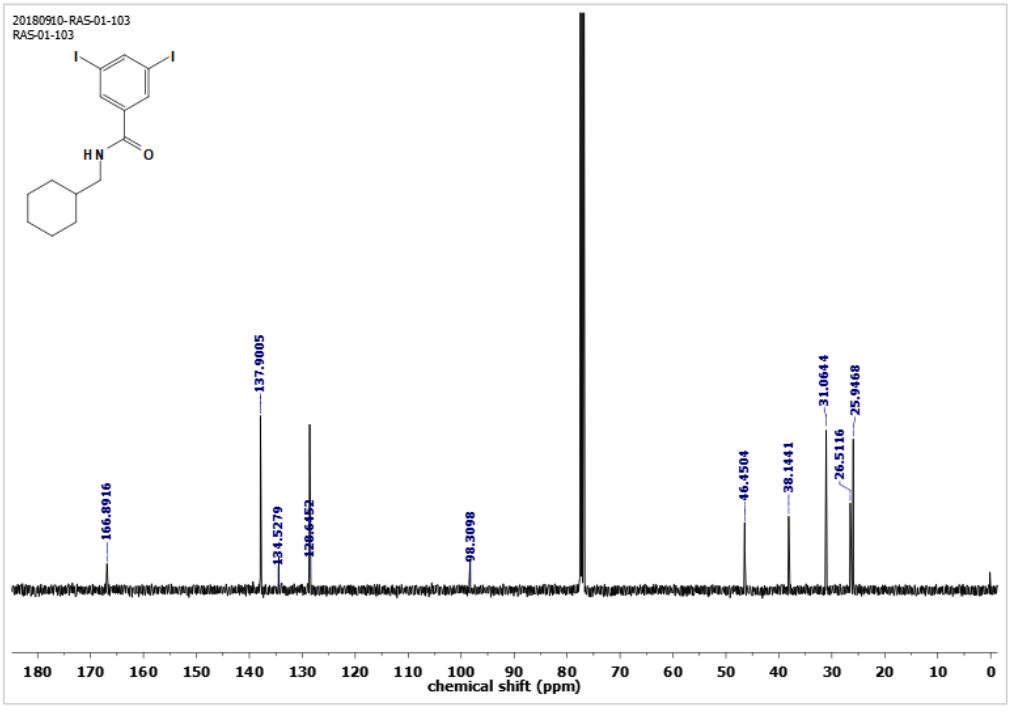

Fig. S24 ^{13}C NMR (101 MHz) spectrum of **5** in $CDCl_3$.

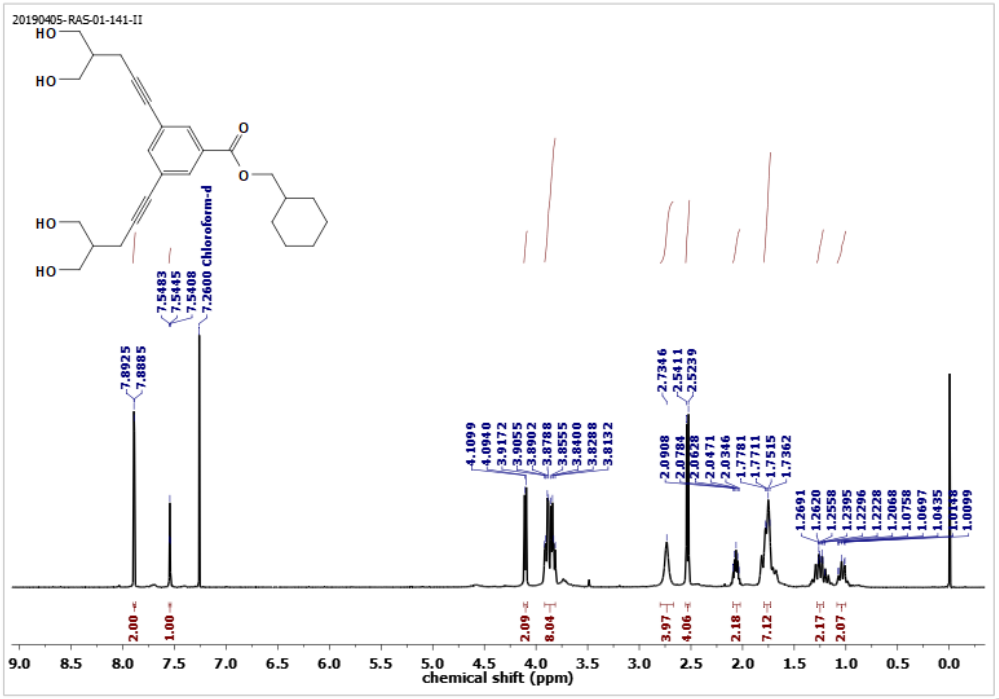

Fig. S25 ^{1}H NMR (400 MHz) spectrum of **1** in $CDCl_3$.

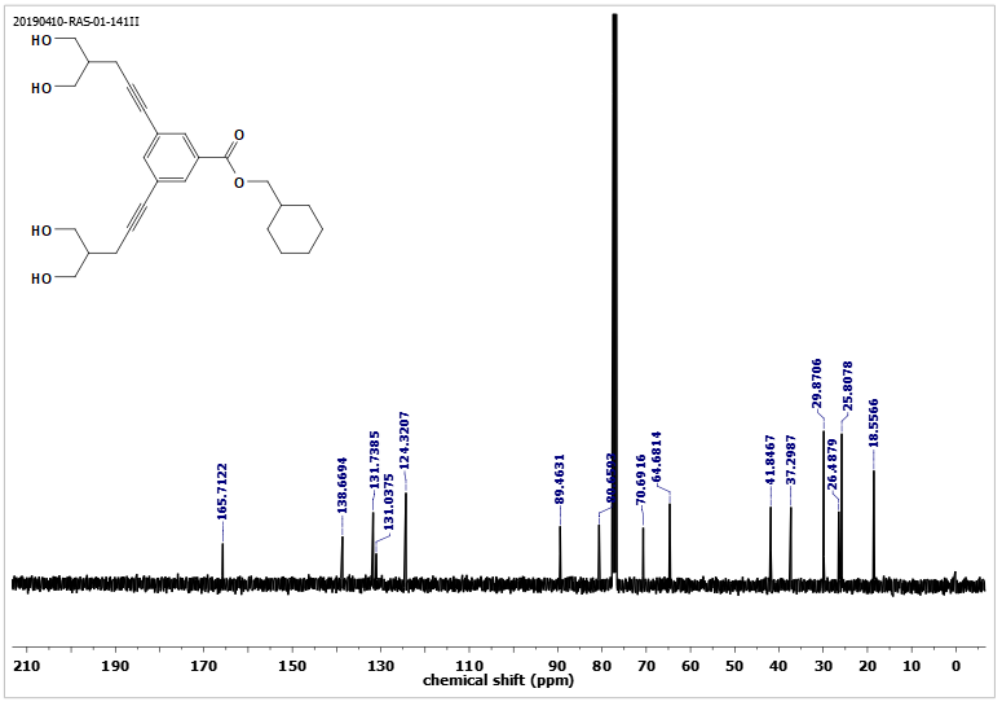

Fig. S26 ^{13}C NMR (101 MHz) spectrum of **1** in $CDCl_3$.

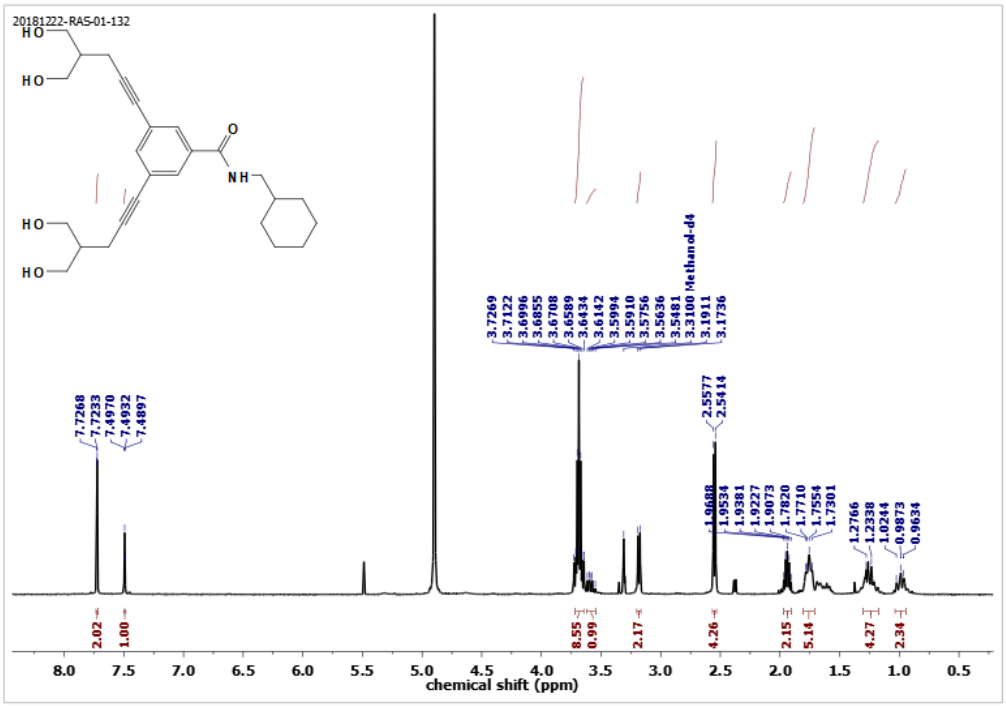

Fig. S27 ^{1}H NMR (400 MHz) spectrum of **2** in MeOH–d_4.

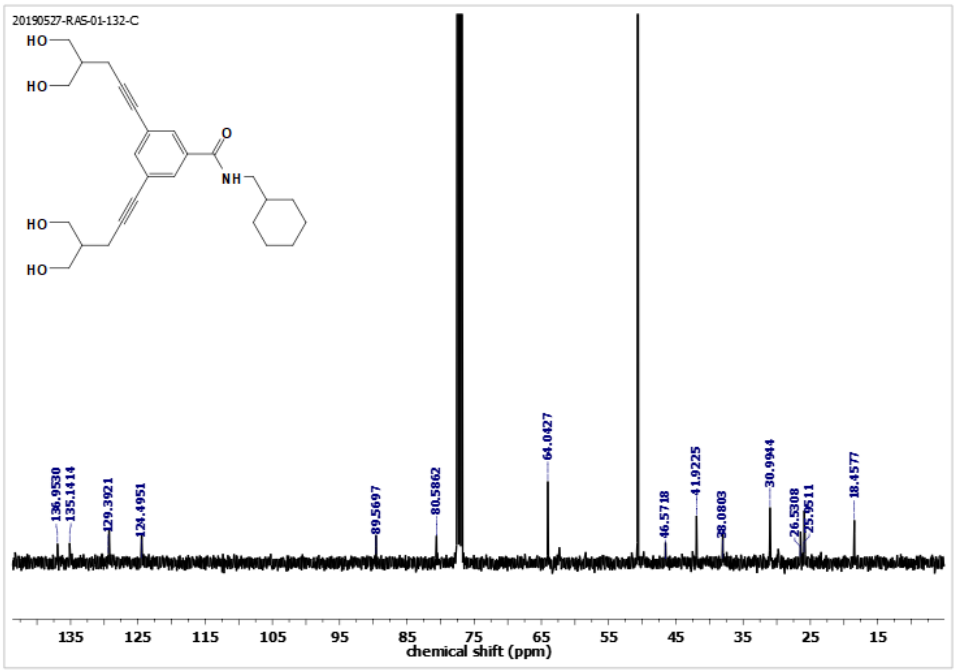

Fig. S28 ^{13}C NMR (101 MHz) spectrum of **2** in $CDCl_3$.

IX. References

S1 J. Mandal, S. Prasad, D. S. Rao, and S. Ramakrishnan, *J. Am. Chem. Soc.*, 2014, **136**, 2538−2545.

S2 M. Banno, T. Yamaguchi, K. Nagai, C. Kaiser, S. Hecht, and E. Yashima, *J. Am. Chem. Soc.*, 2012, **134**, 8718−8728.

S3 D. Tadica, J. Lindersa, J. Andersonb, A. Jacobson and K. Rice, *Tetrahedron*, 2003, **59**, 4603–4614.

S4 N. Fresno, M. González, A. Zaguirre, M. Cuevas, P. Camacho, J. Elguero, F. Pavón, F. Fonseca, P. Goya, and R. Fernández, *J. Med. Chem.*, **2015**, 58, 6639−6652.

S5 U. Dutta, S. Maity, R. Kancherla, and D. Maiti, *Org. Lett.*, **2014**, 16, 6302−6305.

S6 SAINT Plus, (Version 7.03); Bruker AXS Inc.: Madison, WI, 2004.

S7 G. M. Sheldrick, SHELXTL, Reference Manual: version 5.1: Bruker AXS; Madison, WI, 1997.

S8 G. M. Sheldrick, Acta Crystallogr. Sect. A, 2008, 112.

S9 WINGX version 1.80.05 Louis Farrugia, University of Glasgow.

S10 A. L. Spek, A PLATON, Multipurpose Crystallographic Tool, Utrecht University, Utrecht, The Netherlands, 2005.

S11 a) T. Saha, S. Dasari, D. Tewari, A. Prathap, K. M. Sureshan, A. K. Bera, A. Mukherjee and, P. Talukdar, *J. Am. Chem. Soc.*, 2014, **136**, 14128–14135; b) P. Talukdar, G. Bollot, J. Mareda, N. Sakai and S. Matile, *J. Am. Chem. Soc.*, 2005, **127**, 6528–6529; c) V. Gorteau, G. Bollot, J. Mareda, A. Perez-Velasco and S. Matile, *J. Am. Chem. Soc.*, 2006, **128**, 14788–14789.

S12 a) A. Vargas Jentzsch, D. Emery, J. Mareda, P. Metrangolo, G. Resnati and S. Matile, *Angew. Chem., Int. Ed.*, 2011, **50**, 11675–11678; b) https://medical-dictionary.thefreedictionary.com/antiport.

S13 S. Bhosale and S. Matile, *Chirality*, 2006, **18**, 849–856.

S14 A. Roy, D. Saha, A. Mukherjee and P. Talukdar, *Org. Lett.*, 2016, **18**, 5864–5867.

S15 N. Sordé and S. Matile, *J. Supramol. Chem.*, 2002, **2**, 191–199.

S16 P. Talukdar, N. Sakai, N. Sordé, D. Gerard, V. M. F. Cardona and S. Matile, *Bioorg. Med. Chem.*, 2004, **12**, 1325–1336.

S17 N. Busschaert, L. E. Karagiannidis, M. Wenzel, C. J. E. Haynes, N. J. Wells, P. G. Young, D. Makuc, J. Plavec, K. A. Jolliffe and P. A. Gale, *Chem. Sci.*, 2014, **5**, 1118–1127.

S18 M. Lisbjerg, H. Valkenier, B. M. Jessen, H. Al-Kerdi, A. P. Davis, and M. Pittelkow, *J. Am. Chem. Soc.* 2015, **137**, 4948–4951.

S19 D. Mondal, A. Sathyan, S. V. Shinde, K. K. Mishra, P. Talukdar, *Org. Biomol. Chem.,* 2018, **16**, 8690−8694.

S20 L. Rose and A. T. A. Jenkins, *Bioelectrochemistry,* 2007, **70**, 387–393.

S21 C. Ren, X. Ding, A. Roy, J. Shen, S. Zhou, F. Chen, S. F. Yau Li, H. Ren, Y. Y. Yang, H. Zeng, *Chem. Sci.*, 2018, **9**, 4044–4051.

S22 H. J. C. Berendsen, J. P. M. Postma, W. F. van Gunsteren and J. Hermans, (1981) Interaction models for water in relation to protein hydration. In: B. Pullman, Ed., Intermolecular Forces, D. Reidel Publishing Company, Dordrecht, 331–342.

S23 J. Domański, P. J. Stansfeld, M. S. P. Sansom, O. Beckstein, *J. Membr. Biol.*, 2010, **236**, 255–258.

S24 C. Kandt, W. L Ash, D P. Tieleman, *Methods,* 2007, **41**, 475–488.

S25 A. K Malde, L. Zuo, M. Breeze, M. Stroet, D. Poger, P. C Nair, C. Oostenbrink, A. E Mark, *J. Chem. Theory Comput.*, 2011, **7**, 4026–4037.

S26 C. Oostenbrink, A. Villa, A. E. Mark, and W. F. Van Gunsteren, *J. Comput. Chem.*, 2004, **25**, 1656–1676.

S27 B. Hess, C. Kutzner, D. van der Spoel, and E. Lindahl, *J. Chem. Theory Comput.*, 2008, **4**, 435–447.

S28 S. Nosé, *Molecular Physics*, 1984, **52**, 255–268.

S29 M. Parrinello, and A. Rahman, *J. Appl. Phys.*, 1981, **52**, 7182–7190.

S30 T. Darden, D. York, and L. Pedersen, *Chem. Phys.*, 1993, **98**, 10089–10092.

S31 P. Raiteri, A. Laio, F. L. Gervasio, C. Micheletti, and M. Parrinello, *J. Phys. Chem.*, 2006, 110, 3533–3539.